Integration of thermochemical water splitting with CO_2 direct air capture

Casper Brady[a], Mark E. Davis[b,1], and Bingjun Xu[a,1]

[a]Center for Catalytic Science and Technology, Chemical and Biomolecular Engineering, University of Delaware, Newark, DE 19716; and [b]Chemical Engineering, California Institute of Technology, Pasadena, CA 91125

Contributed by Mark E. Davis, October 18, 2019 (sent for review September 13, 2019; reviewed by Christopher W. Jones and Steven Suib)

Renewable production of fuels and chemicals from direct air capture (DAC) of CO_2 is a highly desired goal. Here, we report the integration of the DAC of CO_2 with the thermochemical splitting of water to produce CO_2, H_2, O_2, and electricity. The produced CO_2 and H_2 can be converted to value-added chemicals via existing technologies. The integrated process uses thermal solar energy as the only energy input and has the potential to provide the dual benefits of combating anthropogenic climate change while creating renewable chemicals. A sodium–manganese–carbonate (Mn–Na–CO_2) thermochemical water-splitting cycle that simultaneously drives renewable H_2 production and DAC of CO_2 is demonstrated. An integrated reactor is designed and fabricated to conduct all steps of the thermochemical water-splitting cycle that produces close to stoichiometric amounts (~90%) of H_2 and O_2 (illustrated with 6 consecutive cycles). The ability of the cycle to capture 75% of the ~400 ppm CO_2 from air is demonstrated also. A technoeconomic analysis of the integrated process for the renewable production of H_2, O_2, and electricity, as well as DAC of CO_2 shows that the proposed scheme of solar-driven H_2 production from thermochemical water splitting coupled with CO_2 DAC may be economically viable under certain circumstances.

sodium manganese oxide | process integration | technoeconomic analysis

Anthropogenic climate change is increasingly recognized as a serious and imminent threat to the prosperity of human society. A recent Intergovernmental Panel on Climate Change report claims that human activities have caused ~1 °C increase in global warming, and that net zero global CO_2 emissions is needed to cap the warming below 1.5 °C in the next few decades to avoid catastrophic consequences (1). Even if drastic measures are taken to completely halt anthropogenic CO_2 emissions by 2040, negative effects of high atmospheric CO_2 concentration [415 ppm as of May 2019 (2)] will still persist for decades afterward (1) due to the long lifetime of atmospheric CO_2 [thousands of years (3)]. Thus, it is not only imperative to reduce CO_2 emissions, but also to consider actively removing CO_2 from the atmosphere via direct air capture (DAC). Temperature/humidity swing adsorption with liquid amines, e.g., monoethanolamine (4, 5), is widely practiced in the natural gas industry and has been proposed for CO_2 removal from the flue gas of coal-fired power plants (6–8). The majority of the most mature DAC processes are based on amine adsorbents (9); however, several undesirable features, such as low stability to oxygen environments at elevated temperatures of CO_2 removal (4), make the search for alternative adsorbents necessary. Aqueous alkali hydroxides have been proposed as absorbents in DAC processes very similar to the Kraft Caustic Recovery Cycle commonly used in the paper mill/pulp industry (10) (left cycle in Fig. 1). In these processes, dilute CO_2 in air is absorbed to form carbonate ions in an aqueous solution of an alkali hydroxide (Na^+ or K^+) via an acid–base reaction, followed by the introduction of calcium hydroxide to separate the carbonate in the form of solid calcium carbonate precipitate and regenerate the initial alkali hydroxide solution. The calcium carbonate is then calcined at high temperatures (600–900 °C) to produce a CO_2 stream and calcium oxide ready for use in the subsequent cycle (after reacting with water to form calcium hydroxide), thus completing the cycle (*SI Appendix*, Table S1). Two metal cations must be used in the cycle due to the different properties of the hydroxide and carbonate of $Na^+(K^+)$ and Ca^{2+}. The low solubility of $Ca(OH)_2$ in water makes it unsuitable as an absorbent, while the high thermal stability of K_2CO_3 and Na_2CO_3 makes their thermal decomposition energetically unfavorable (11). Despite recent research efforts, existing DAC processes have economics that could stand improvement (100–500 $/ton CO_2) (4, 9, 12–14). A comprehensive technoeconomic analysis of current DAC technologies is available (14).

We recently developed a thermochemical water-splitting (TWS) cycle based on a Mn–Na–CO_2 reaction network that is capable of splitting water into stoichiometric amounts of hydrogen and oxygen in 3 reaction steps, the highest temperature step operating at 850 °C (15). In contrast to sulfur–iodine TWS cycles (16, 17), no toxic/corrosive chemicals are involved in the Mn–Na–CO_2 system. The thermodynamic driving force of this TWS cycle is based on the divergent thermal and chemical stabilities of different manganese oxide species (α-$NaMnO_2$ and MnO_x) at different temperatures and environments (*SI Appendix*, Table S1 and Fig. S1) (15). A key step of interest in the context of DAC in this cycle is the extraction of Na^+ from MnO_x layers of α-$NaMnO_2$ with CO_2 to form H_xMnO_y and Na_2CO_3. α-$NaMnO_2$ slurries are quite alkaline in nature (pH = 12–13), making them attractive as potential CO_2 adsorbents. There are 2 key parallels between the Mn–Na–CO_2 TWS and the Kraft cycles: 1) the use of CO_2 as an acid to extract alkali cations from an alkaline compound (α-$NaMnO_2$ and NaOH/KOH, blue in both cycles in Fig. 1), and 2) high-temperature production of CO_2 via thermal decomposition of

Significance

Global warming as a result of rising atmospheric CO_2 concentrations is considered an imminent threat to society. In order to address rising CO_2 concentrations, effective CO_2 capture directly from the atmosphere is likely to be necessary. We integrate direct air capture CO_2 and water splitting to produce a mixture of CO_2 and H_2 via a thermochemical water-splitting cycle. This mixture can, in turn, be used to produce valuable chemicals by known technologies. We demonstrate via experimental investigations and a technoeconomic analysis that the demonstrated integration of the 2 technologies into a single overall process has the potential to become economically favorable in some situations.

Author contributions: C.B., M.E.D., and B.X. designed research; C.B. performed research; C.B., M.E.D., and B.X. analyzed data; and C.B., M.E.D., and B.X. wrote the paper.

Reviewers: C.W.J., Georgia Tech; and S.S., University of Connecticut.

The authors declare no competing interest.

[1]To whom correspondence may be addressed. Email: mdavis@cheme.caltech.edu or bxu@udel.edu.

This article contains supporting information online at https://www.pnas.org/lookup/suppl/doi:10.1073/pnas.1915951116/-/DCSupplemental.

First published November 21, 2019.

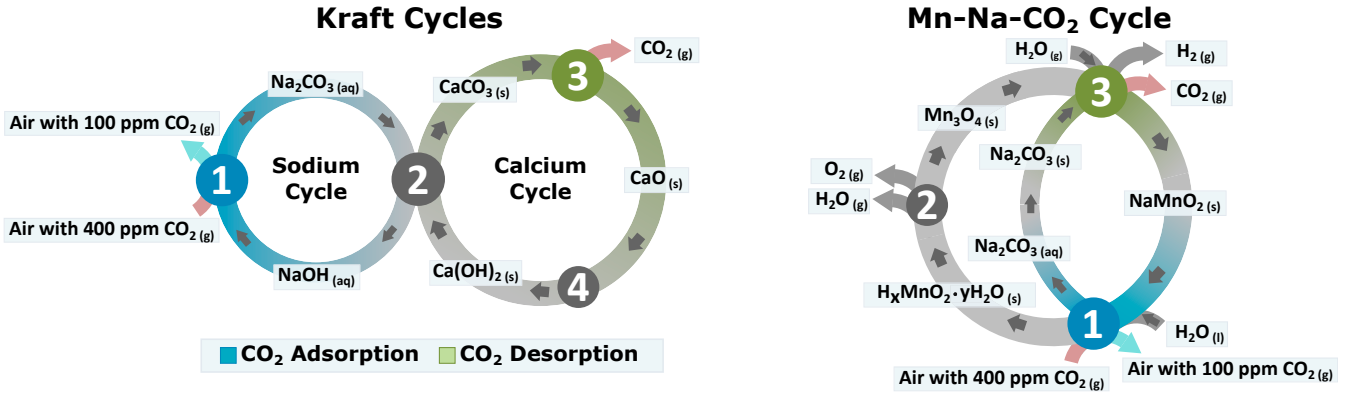

Fig. 1. Schematics of Kraft process based cycles present in literature and the Mn–Na–CO_2 water-splitting cycle as a CO_2 capture process. All reactions in both cycles are included in *SI Appendix*, Tables S1 and S2.

carbonates (Na_2CO_3 and $CaCO_3$, green in Fig. 1). These 2 parallels suggest that the Mn–Na–CO_2 TWS cycle has the potential to enable simultaneous DAC of CO_2 and hydrogen production.

In this work, we demonstrate a methodology that integrates the DAC of CO_2 and thermochemical water splitting that produces a mixture of CO_2 and H_2 (Fig. 2). The CO_2/H_2 stream can be converted to a variety of fuels and chemicals, e.g., to syngas via the reverse water–gas shift reaction (18, 19) or methanol via a number of established catalytic processes (20). Alternatively, the CO_2/H_2 stream can be directly upgraded to higher hydrocarbons via a number of established processes (18, 21). In this work we limit our analysis to CO_2 capture and water splitting without considering the economics of further upgrading in order to avoid added complexity and to allow our process to be directly compared to other DAC technologies.

Results and Discussion

Process Design and Implementation. While the chemistry of all 3 steps in the Mn–Na–CO_2 cycle has been established (15), several major challenges remain in coupling the cycle with a solar thermal power source and the DAC of CO_2: 1) solar energy is inherently intermittent, restricting the amount of time high-temperature reactions can be performed, and 2) DAC of CO_2 requires the utilization of massive airflow. Here, we a provide a solution to these issues (summarized in Fig. 3). Heat for the cycle is supplied by a solar collector field that provides superheating steam at 1,000 °C. Concentrated solar thermal power is useful for generating high-quality heat for water-splitting cycles (22, 23). However, the diurnal cycle of available solar energy restricts the amount of time a water-splitting reactor can be held at high temperatures on a daily basis. Conveniently, the combined water splitting and CO_2 DAC process has 2 distinct operating regimes that pair well with this diurnal constraint. While high-quality heat is required for the high-temperature steps, sodium extraction is exothermic and time-consuming if dilute atmospheric CO_2 is used as a CO_2 source. Thus, cyclic quasibatch operation (*SI Appendix*, Fig. S2 shows a schedule of operation) where the high-temperature steps are performed during the day and Na^+ extraction is performed at night enables effective utilization of reactor time despite the limitations imposed by a diurnal power source. CO_2 DAC requires large flowrates of air due to the low concentration (~400 ppm) of CO_2. This leads to a correspondingly large power requirement. We address this issue by utilizing a solar updraft tower (24, 25). These systems have been proposed since the late 1990s for generating power from solar heating via thermal updraft through a power-generating turbine suspended in a large tower surrounded on ground level by a large solar collection basin (Fig. 3, *Left*). While this technology usually shows low efficiency in producing electricity (24), it is an excellent source of high flowrates of air without the corresponding electricity costs. Large thermal reservoirs are typically included in the base of updraft towers such that the airflow is relatively constant 24 h a day (24). This allows the tower to provide airflow for CO_2 capture at night, while also producing electricity during the day, when large air flowrates are not required. In general, diurnal systems suffer from low throughput and low efficiencies due to poor process intensification (26). We stress that this diurnal quasibatch operating schedule is only 1 possible implementation of this concept. With the implementation of a high-temperature heat storage system (27) and/or a system for the recirculation of solids (13) the cycle could be executed with higher frequencies or even continuously. We evaluate only our diurnal process in this work in order to simplify the necessary process assumptions.

The integration of these 2 passive solar technologies with the Mn–Na–CO_2 water-splitting cycle yields a process ideal for coupling DAC of CO_2 and water splitting. High-temperature steps that produce hydrogen and oxygen operate during the daytime when concentrated solar energy is available with steam as a heating medium (Fig. 3, *Top Right*). The heat exchange/separation system (Fig. 3, *Bottom Right*) receives either dilute streams of H_2 and CO_2 in steam (during the H_2 evolution step) or O_2 in steam (during the thermal reduction step) from the TWS reactor. These steps are separated by either the introduction of Na_2CO_3 or sodium extraction, such that these 2 gas streams are produced in distinct time periods throughout the cycle. This gas stream is first cooled to ~600 °C in a heat exchanger that provides heat to dry Na_2CO_3 solutions produced during sodium extraction. This 600 °C stream is then introduced to a steam turbine that cools the stream further to 100 °C and produces electricity. A water knockout vessel is used to condense the majority of the steam and separate the final gas

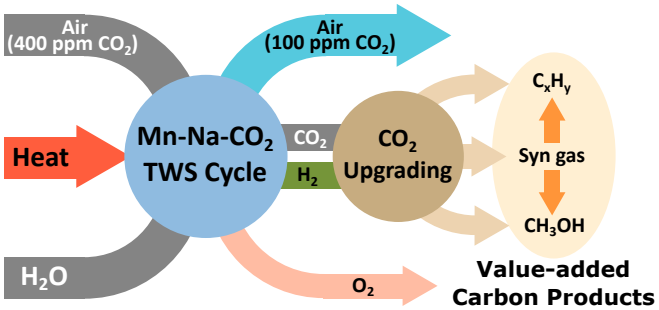

Fig. 2. An overall schematic of the integrated process for DAC of CO_2 and thermochemical water splitting.

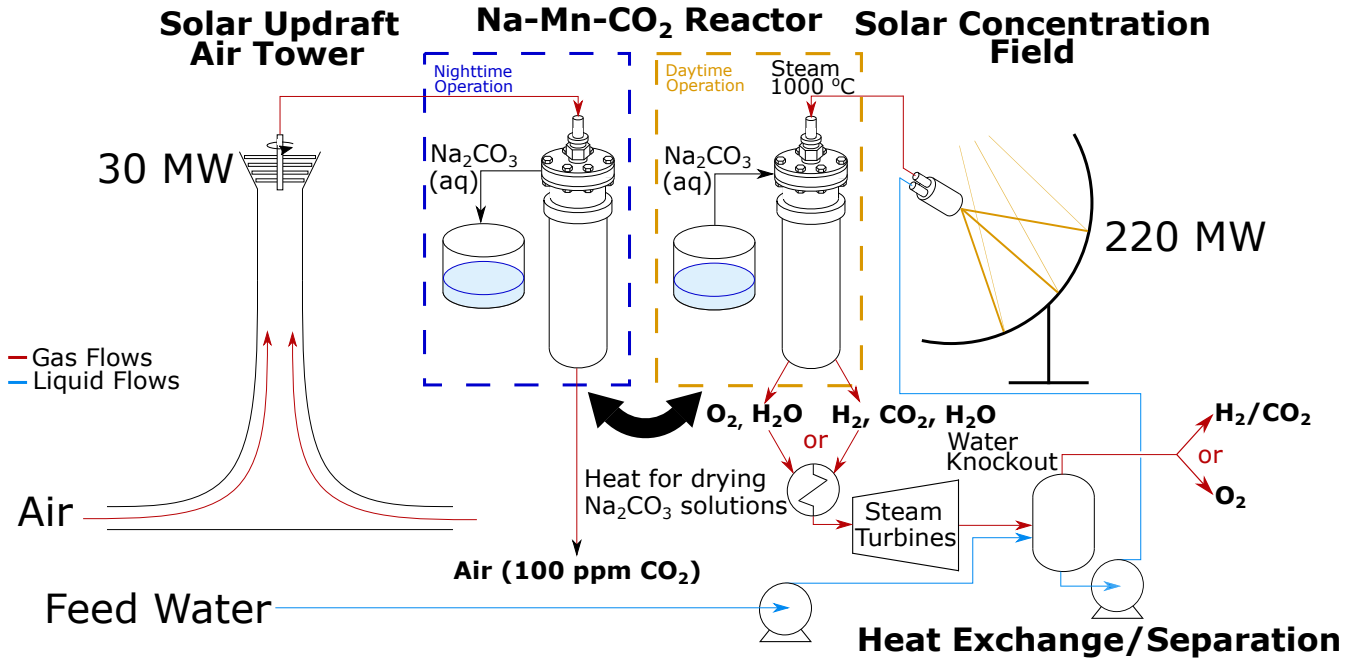

Fig. 3. A schematic of the proposed integrated DAC and TWS process.

mixture (H_2 and CO_2 or O_2). The condensed water can then be reused as a source of steam such that each cycle consumes only the stoichiometric amount of water for water splitting. The use of steam as a reactant, heat-transfer medium, and carrier gas significantly simplifies the process as compared to other water-splitting cycles that require inert carrier gases (28, 29) and makes leveraging waste heat (via steam turbine) possible. At night, liquid water is supplied to the water-splitting reactor and a constant flow of air from the solar updraft tower (heat captured during the day by the solar tower allows operation at night; 24-h operation of solar towers is already proven in other applications) is introduced in order to extract sodium from α-$NaMnO_2$ via CO_2 absorption. At the end of the night the resulting Na_2CO_3 slurry is removed and dried during the day using excess heat from the TWS reactor effluent. The dried solid is then reintroduced to the TWS reactor between thermal reduction and H_2 evolution via solid–gas fluidization. This design yields a process that requires only water, air and sunlight to produce a stream of concentrated CO_2 and H_2 for further upgrading, a stream of pure oxygen, and electricity. It should be noted that pure H_2 and CO_2 streams can also be produced with this TWS if necessary.

Reactor Design. We designed and fabricated an integrated reactor for the Mn-Na-CO_2 TWS cycle to demonstrate its feasibility. In our previous work, we elucidated the chemistry of each step in Mn–Na–CO_2 TWS in separate reactors on a test-tube scale (~200-mg solid) (15). A key challenge in the implementation of this cycle is the drastically different operating conditions, i.e., solid–gas phase reactions at 850 °C for hydrogen and oxygen evolutions, and solid–liquid phase Na^+ extraction and CO_2 capture at 90 °C. The fabricated reactor eliminates the necessity of movement of solids with a capacity of handling ~10-g solid, which is a 50-fold increase from our initial work (*SI Appendix*, Fig. S3, details provided in *Experimental Procedures*). The reactor consists of an alumina vessel with multiple inlets and outlets to control the flow of liquids and gases into and out of the reaction zone. We demonstrate below that all 3 steps in the Mn–Na–CO_2 TWS cycle can be conducted in the fabricated reactor with close to stoichiometric H_2 and O_2 yields in multiple cycles.

Hydrogen Evolution. During hydrogen evolution, a stoichiometric mixture of Mn_3O_4 and Na_2CO_3 (2:3 molar ratio) is initially heated to 850 °C under an inert gas flow and then under steam to form $NaMnO_2$, CO_2, and H_2. Prior to the introduction of steam (Fig. 4*A*, i), the only gas-phase product formed as the solid mixture is heated to 850 °C is CO_2. This reaction leads to the formation of a 2:1 ratio of α-$NaMnO_2$ and MnO as we have shown in our previous work (15). No oxidation state change of manganese occurs in this step, as Mn^{III} and Mn^{II} in Mn_3O_4 form α-$NaMnO_2$ and MnO, respectively. Upon introduction of steam to the solid mixture at 850 °C at the end of 5 h (Fig. 4*A*, ii), MnO is oxidized by water in the presence of unreacted Na_2CO_3 to form additional α-$NaMnO_2$, and a mixture of H_2 and CO_2 with a molar ratio of 1:1.

Sodium Extraction. Na^+ intercalated in the MnO_x layers of α-$NaMnO_2$ must be removed before Mn_3O_4 can be thermally reduced to complete the TWS cycle. Sodium extraction is performed by cooling the solids produced in the hydrogen evolution step to 90 °C, followed by the introduction of water to the reactor via the liquid inlet and bubbling of 5% CO_2 in N_2 via the gas inlet into the liquid–solid slurry. Initially complete CO_2 absorption is observed (Fig. 4*B*), demonstrating the high binding affinity of Na^+ to CO_3^{2-} and facile sodium extraction from the birnessite phase formed upon contact of α-$NaMnO_2$ with liquid water (30). A detectable amount of CO_2 is observed after 2.3 h in the breakthrough curve, followed by a quick increase of the CO_2 concentration to the level in the feed. Periodic pH measurements of the slurry during extraction reveal that the slurry is very alkaline in nature, with an initial pH of 12.8, that decreases gradually as CO_2 in adsorbed into the liquid. This indicates that Na^+ is gradually extracted from the birnessite phase by CO_2. The onset of incomplete CO_2 adsorption occurs when the pH of the slurry decreases to ~11.4, that corresponds to ~63% of Na^+ extracted based on the amount of CO_2 absorbed. The final pH of the slurry is ~9.6, which is roughly consistent with the formation of a Na_2CO_3–$NaHCO_3$ buffer (31) after the majority of Na^+ has been extracted from the solid. Upon the completion of sodium extraction, the Na_2CO_3–$NaHCO_3$ solution is extracted from the liquid outlet equipped with an inline filter.

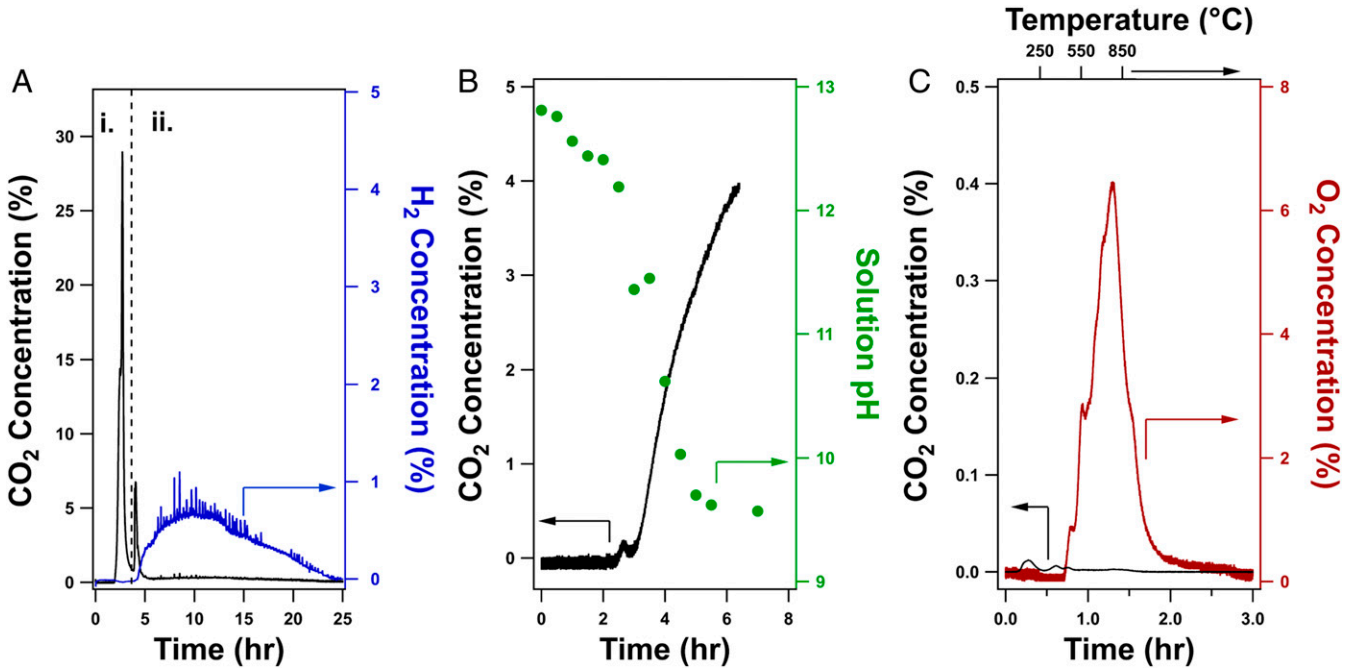

Fig. 4. Gas-phase composition data for the 3 steps in the water-splitting cycle: (*A*) Hydrogen evolution (in *i* dry N_2 is fed; in *ii* a mixture of steam and N_2 is fed), (*B*) sodium extraction, and (*C*) thermal reduction.

Thermal Reduction. The solid component remaining in the reactor from the sodium extraction step is dried and heated to 850 °C to regenerate Mn_3O_4. O_2 is produced during the temperature ramp and hold (Fig. 4*C*) due to the thermal reduction of manganese oxides produced in the previous step to Mn_3O_4 (15). Additionally, a negligible amount of CO_2 is also produced during this step via decomposition of $MnCO_3$ [formed during sodium extraction (15)] during heating. Higher amounts of CO_2 formation were observed in our previous work (15). The difference may be due to the significantly higher α-$NaMnO_2$ weight percentage in the slurry during sodium extraction (~15 wt %) employed in this work, as compared to our previous work (~5 wt %) (15). Sodium extraction takes place via competing redox extraction ($2\ NaMnO_2 + 4\ H^+ \rightarrow Mn^{IV}O_2 + Mn^{2+} + 2\ Na^+ + 2\ H_2O$) and ion exchange ($NaMn^{III}O_2 + H^+ \rightarrow HMn^{III}O_2 + Na^+$) where the redox mechanism dominates at low pH (32). $MnCO_3$ formation is attributed to the reaction between the aqueous Mn^{2+} formed via the redox mechanism and CO_2 (15). Thus, higher weight loadings of α-$NaMnO_2$ in the slurry suppress the redox mechanism by maintaining a higher pH, which in turn reduces the $MnCO_3$ formation. It is desirable for CO_2 evolution to only take place during the H_2 production step as mixtures of CO_2 and H_2 are valuable while mixtures of CO_2 and O_2 would require costly separation. At the end of the thermal reduction step, the reactor is cooled to ~100 °C, followed by the introduction of a Na_2CO_3 solution. Evaporating the water yields a solid mixture of Na_2CO_3 and Mn_3O_4 ready for the hydrogen evolution step in the subsequent cycle.

Overall Cycling Performance. Near-theoretical yields of H_2 and O_2 are produced from the Mn–Na–CO_2 TWS cycle in the fabricated reactor over the course of 6 consecutive cycles (Fig. 5*A*). A stoichiometric mixture of Mn_3O_4/Na_2CO_3 is charged in the reactor prior to the hydrogen evolution step of the first cycle, and no additional manganese oxide is added to or removed from the reactor in all consecutive cycles. Roughly 90% of the theoretical amounts of H_2 and O_2 are produced in each cycle (Fig. 5*A*) with no discernible decrease in production with increasing cycles. The lack of deactivation is in part due to the fact that complete phase change is involved in every step, e.g., the intercalation of Na^+ into and extraction of Na^+ from MnO_x layers (15). Thus, each cycle has a fresh start without any "memory" from previous cycles. Further, roughly 90% of the stoichiometric amount of CO_2 is produced in the hydrogen evolution step in each cycle (Fig. 5*B*), with a negligible amount of CO_2 produced in the thermal reduction step. Powder X-ray diffraction patterns of solids after all 3 steps in the 6th cycle were collected (*SI Appendix*, Fig. S4*A*) and the data confirm that the expected phases are formed based on our previous work (15). Analysis of the X-ray diffraction patterns of produced Mn_3O_4 at several points in the cycle (*SI Appendix*, Fig. S4*B*) reveals that the average particle size decreases slightly during the 6-cycle test. Typically, $CaO/CaCO_3$ particles in Kraft-based cycles increase in size dramatically over the course of many cycles, limiting practical reuse (13). The fact that our Na–Mn–CO_2 system does not suffer from the same issue may allow substantially longer times between the replacement of solids. Results from these cycling experiments demonstrate that the fabricated reactor can be used to facilitate the Mn–Na–CO_2 TWS cycle.

DAC of CO_2 with Mn–Na–CO_2 TWS Cycle. The alkaline nature of aqueous suspensions of α-$NaMnO_2$ (Fig. 4*B*) suggests that it could be an effective adsorbent for CO_2 DAC. To evaluate the feasibility of this we employ ambient air with ~400 ppm of CO_2 as a CO_2 source to extract sodium from α-$NaMnO_2$ rather than 5% CO_2 that was used in our cycling test. The breakthrough curves for CO_2 absorption in several α-$NaMnO_2$ slurries with varying $NaMnO_2$ loadings (Fig. 6*A*) show an excellent initial performance, absorbing more than 75% of CO_2 from air. The fraction of sodium extracted by CO_2 before the air effluent contains more than 100 ppm of CO_2 increases (up to 72%) with the amount of α-$NaMnO_2$ in the slurry (Fig. 6*B*). This is likely a consequence of the lower initial pH of slurries with low weight loading of α-$NaMnO_2$ (0.2–0.8 wt %) caused by near-complete extraction of Na^+ from the $NaMnO_2$ layers upon initial introduction of water. In contrast, ~15 wt % of $NaMnO_2$ slurry in water is used in the cycling experiments. The primary reason to use a relatively low $NaMnO_2$ wt % slurry in the proof of concept CO_2 DAC experiments is to measure these

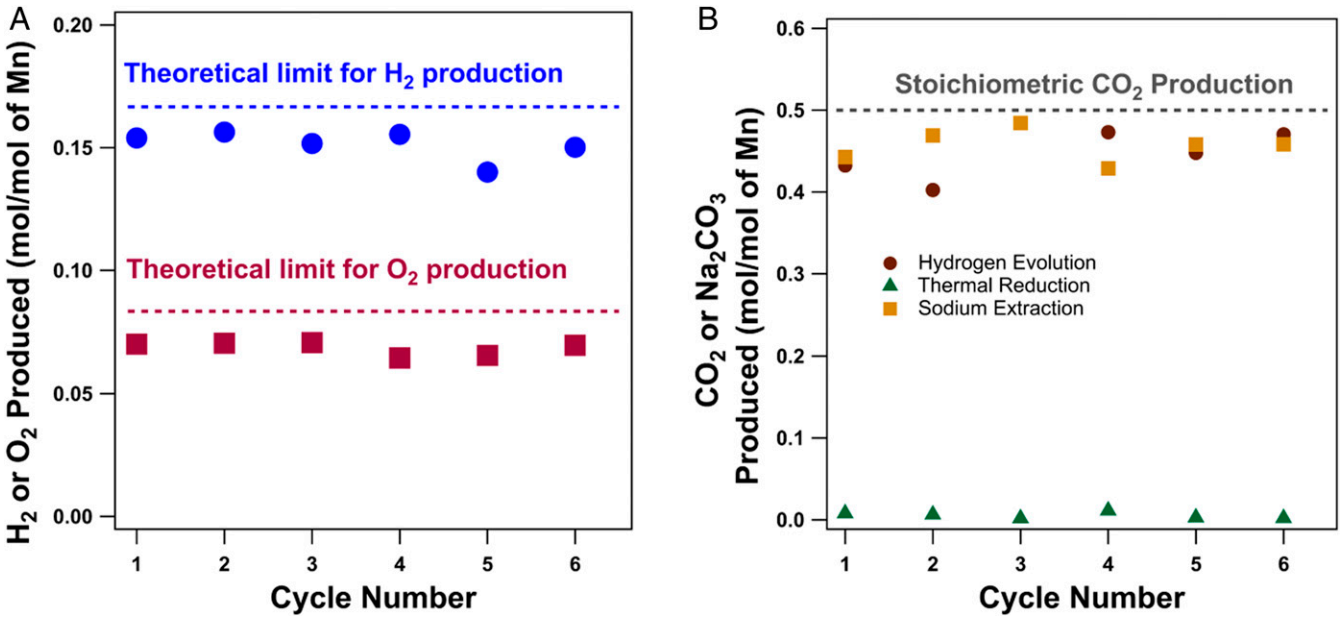

Fig. 5. Amounts of (*A*) H_2 and O_2 produced, and (*B*) CO_2 captured/produced in 6 consecutive TWS cycles. All gas products are quantified with an SD of ~4%.

breakthrough curves in reasonable timescales. The amount of CO_2 captured when the CO_2 concentration in the effluent recovers to 400 ppm is in all cases consistent with ~90% of intercalated Na^+ being converted to Na_2CO_3 (similar to the case when 5% of CO_2 is used). As the weight fraction of $NaMnO_2$ in the slurry increases, the fraction of Na^+ extracted before the effluent air contains more than 100 ppm of CO_2 is expected to increase.

Technoeconomic Analysis. A preliminary technoeconomic analysis is performed on a large-scale design based on the proposed flowsheet (Fig. 3) on a plant that removes 25,000 metric tons of CO_2 from the atmosphere per year. The major unit processes used are 1) a water-splitting reactor, 2) a field of heliostats focused on a central tower, 3) a solar updraft tower to generate the airflow during Na^+ extraction at night and provide electricity during the day, and 4) a series of steam turbines to utilize waste heat in cooling the water-splitting effluent. The system is simulated as a quasibatch system where a water-splitting reactor is cycled through all of the required steps of the cycle once a day, performing the high-temperatures step during the day and the low-temperature step at night (*SI Appendix*, Fig. S2). In order to determine the extent to which integration of the updraft tower and steam turbines affects the feasibilities of the plant, we consider 4 alternate cases. Case 1 considers a plant that is not integrated with solar airflow or steam turbines for power recuperation. Case 2 considers a plant that is integrated with a solar updraft tower for airflow and power generation. Case 3 considers the construction of a full plant

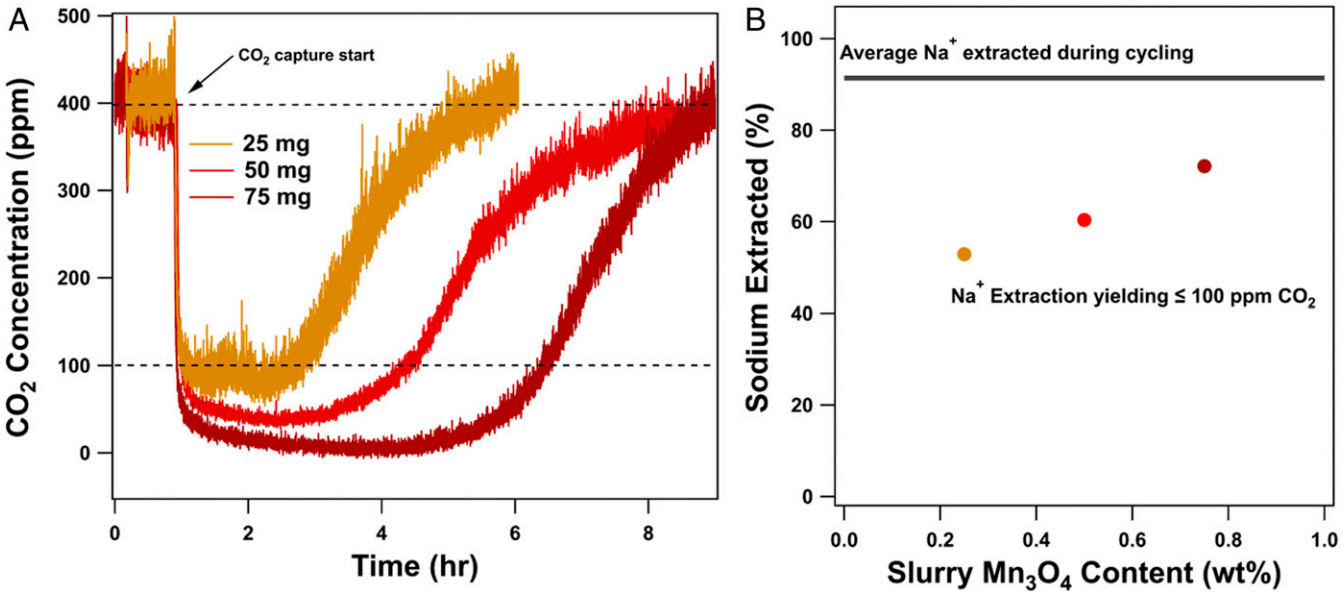

Fig. 6. CO_2 direct air capture experiments: (*A*) CO_2 in air breakthrough curves during DAC tests. (*B*) The fraction of the Na^+ extracted during DAC of CO_2 while CO_2 concentrations are below 100 ppm. All gas products are quantified with an SD of ~4%.

with the implementation of a series of turbines but no solar updraft tower. Case 4 takes into account the implementation of both a solar updraft tower and a series of steam turbines. A detailed account of all 4 cases and all relevant assumptions are provided in *SI Appendix*, Fig. S5. For each case we evaluate the economic viability using an optimistic CO_2 price of $200/ton. Cases 1–3 exhibit negative net present values (NPVs) even at this quite optimistic CO_2 price, highlighting the importance of proper integration of the water-splitting cycle with other technologies for power generation. The NPV of case 4 is dependent on financial assumptions but is positive, assuming a CO_2 price of $200/ton. Thus, we focus on the fully integrated system for further analysis.

The total costs of the fully integrated system investigated in case 4 are dominated by initial capital costs, mainly the solar energy harvesting facilities (Fig. 7*A*). The combination of concentrated solar power, water splitting, CO_2 removal, and turbines to produce electricity makes this process different from other DAC processes in its reliance on several revenue streams (Fig. 7*B*). The generation of H_2, O_2, CO_2, and electricity contributes to the plant's revenue, although the vast majority of the revenue is derived from the generation of electricity. As a result, the economic viability of the proposed process depends on the value of all these outputs (Fig. 7*C*). For example, assuming H_2, O_2, and electricity prices of $2/kg (33), $0.04/kg (34), and $0.167/kWh [average cost of electricity in California in June 2019 (35)], respectively, a CO_2 price of $83/ton is needed for the proposed plant to break even. This hypothetical price point is lower than previous reports (4, 12–14). This relatively low projected break-even CO_2 price illustrates the economic feasibility of such an integrated process, despite its dependence on the assumed electricity price (*SI Appendix*, Fig. S6). It is noted that no carbon subsidy is assumed in the analysis. Due to the nature of the proposed cycle, the degree of uncertainty of the technoeconomic analysis will be greater than those on DAC schemes leveraging years of pilot plant data and vast industrial knowledge on similar processes. Our process is leveraging 2 reasonably mature solar-to-power technologies (updraft towers and solar thermal concentrators coupled to heat engines) to offset the costs of CO_2 DAC via electricity generation; thus, the comparison to processes that aim only to capture CO_2 may not be a fair comparison. Although the current analysis focuses on CO_2 DAC, the proposed cycle can also use more concentrated sources of CO_2, which is expected to yield improved economics as less inlet gas flow is needed for a given amount of CO_2 captured. As the majority of the capital cost of the process is derived from the solar-harvesting facilities, it is expected that as these technologies mature and improve, these costs will decrease. There is precedence in literature for dramatic cost reduction after the construction of a pioneer plant as a result of improvements in manufacturing/experience in both solar-harvesting technologies (36) and for direct air capture (13).

Conclusions

We established the concept of using a Mn–Na–CO_2 water-splitting cycle combined with the DAC of CO_2 to create an integrated methodology that under certain circumstances may be economically viable for the production of renewable chemicals. We have designed a complete process schematic, constructed a 1-vessel test reactor capable of performing a complete TWS cycle, performed proof of concept CO_2 direct air capture tests, and assessed the economic viability of the approach. We have demonstrated that our reactor design can facilitate several cycles of the complete water-splitting reaction system. Direct air capture tests illustrated that alkaline slurries of $NaMnO_2$ could remove CO_2 from air with high efficacy even at ultradilute CO_2 concentrations. While our technoeconomic analysis was preliminary, it demonstrated that the proposed process may be economically feasible for combining CO_2 removal from the atmosphere with thermochemical water splitting to produce a gas stream (CO_2/H_2) that could be readily integrated with existing chemical processes to create renewable chemicals.

Experimental Procedures

Cycling Tests. The experimental test reactor is constructed from readily available parts. The reactor tube is an 8.5-in.-long closed-ended Al_2O_3 tube with an outer diameter of 1 in. and an inner diameter of 0.75 in. The gas-handling and liquid-handling tubes are Al_2O_3 tubes with outer diameters of 1/4 and 1/8 in. and inner diameters of 3/16 and 1/16 in., respectively. All Al_2O_3 tubes are purchased from AdValue Technologies. An Inconel clad thermocouple (Omega) is threaded through the gas-handling tube in order to accurately measure temperatures in the reactor tube. All gas flows are controlled with Brooks mass-flow controllers. Steam is introduced via a Cole Parmer syringe pump with a 60-mL syringe. All other liquid additions or extractions are performed using the reactor syringe port using a Corning 0.20-μm nylon filter as an inline filter. The reactor is heated by a clamshell furnace (Lingberg/Blue M) and the gas distribution section is heated to 150 °C to prevent condensation of steam. All heaters and mass flow controllers are controlled via an integrated LabView program made in-house. An online differentially pumped quadrupole mass spectrometer (Stanford Research Instruments RGA100) is used to quantify gas products and a 100-mL condenser suspended in an ice bath is positioned upstream of the residual gas analyzer (RGA) to remove excess water.

Cycling experiments are performed by first preparing a physical mixture of Mn_3O_4 and Na_2CO_3 (Sigma-Aldrich) via grinding with a mortar and pestle. This mixture is then loaded into the reactor with care so as not to clog the gas-handling tube with solids. The water-splitting step is performed by first heating the physical mixture to 850 °C under a flowrate of 50 sccm of nitrogen at

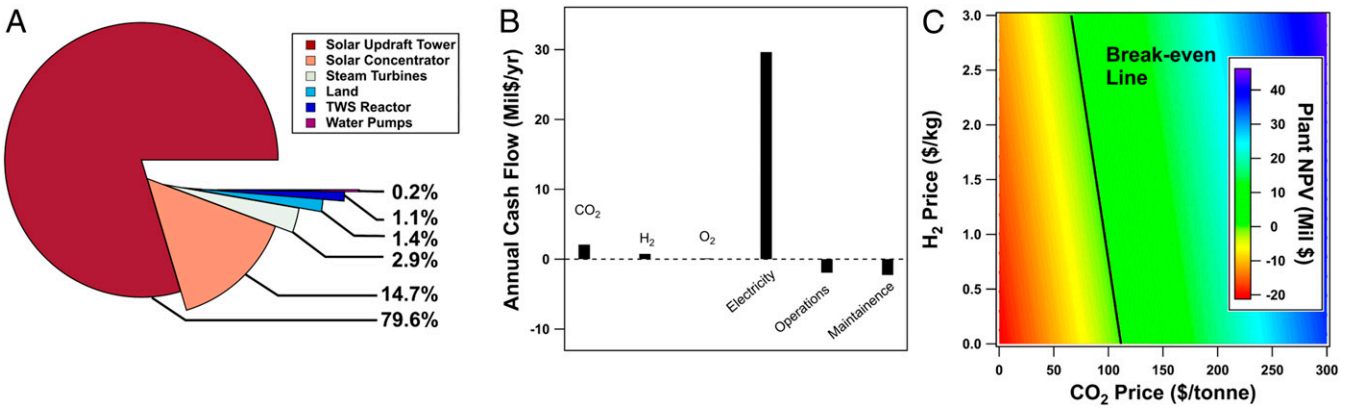

Fig. 7. Technoeconomic analysis of the process: (*A*) A summary of installed costs of major unit processes, (*B*) the annual revenue and costs of operating the DAC and water-splitting process assuming CO_2 is sold at 83 $/ton, and (*C*) the net present value of the process as a function of the selling prices of H_2 and CO_2 (the line represents the prices required for the plant to break even).

a ramping rate of 10 °C/min. After the set temperature is reached, steam is introduced to the heated inlet gas line by syringe pump at a rate of 2 mL/h of liquid. Once the reaction is completed (hydrogen production ceases) the steam flowrate is stopped, and the reactor is cooled to room temperature under nitrogen.

Once cool, sodium extraction is performed. First ~40 mL of deionized (DI) water is introduced to the reactor using the syringe port on the side of the reactor and the reactor is heated to ~80 °C while 50 sccm of N_2 is bubbled through the solution. Once the reactor has reached the set temperature a small flowrate of CO_2 is introduced into the nitrogen carrier gas such that a 5% CO_2 in N_2 stream at 50 sccm is fed to the reactor. The online RGA is used to measure CO_2 concentration during this time to establish a rough degree of extraction. Sodium extraction is performed in 3 steps starting from 5% CO_2 in N_2, 10% CO_2 in N_2, and finally pure CO_2 to insure complete sodium extraction. Between each step ~40 mL of liquid is extracted, filtered, and replaced with the same volume of DI water using the inline filter attached to the syringe port. After the pH of the extracted solution is ~7.5–8 the reactor is heated to and held at 100 °C for several hours to remove the remaining water.

Thermal reduction of the postextraction solid is performed by heating the reactor to 850 °C at a rate of 10 °C/min under a flow of 50 sccm of nitrogen. The RGA is used to quantify produced O_2 and the reactor is cooled once oxygen production ceases. After cooling to room temperature an aqueous solution of Na_2CO_3 is introduced to the reactor via the syringe port and the reactor is heated to 100 °C, removing water and leaving a physical mixture of Mn_3O_4 and Na_2CO_3 which is used in the next cycle.

Air-Scrubbing Tests. Air-scrubbing tests are performed using a small 4-in. closed-end Al_2O_3 tube with an outer diameter of 1 in. and an inner diameter of 0.75 in. A 60-sccm flowrate of air is supplied with a small 5VDC diaphragm pump with a potentiometer to control the flowrate. The same RGA as above is used to track CO_2 concentration during Na extraction. A ppm level CO_2 calibration is obtained for the RGA by diluting atmospheric air with nitrogen in various ratios. $NaMnO_2$ used in tests was synthesized via solid-state synthesis using stoichiometric amounts of Mn_2O_3 (Sigma-Aldrich) and Na_2CO_3 heated in flowing air at 700 °C for 6 h.

Data availability. All data are available in the main text and *SI Appendix*.

ACKNOWLEDGMENTS. C.B. and B.X. acknowledge support from the University of Delaware Research Foundation UDRF-SI 2017.

1. P. J. First, *Global Warming of 1.5 C An IPCC Special Report on the Impacts of Global Warming of 1.5 C Above Pre-Industrial Levels and Related Global Greenhouse Gas Emission Pathways, in the Context of Strengthening the Global Response to the Threat of Climate Change, Sustainable Development, and Efforts to Eradicate Poverty*. https://www.ipcc.ch/sr15/. Accessed 1 October 2019.
2. P. Tans, R. Keeling, Data from "Trends in atmospheric carbon dioxide." https://www.esrl.noaa.gov/gmd/ccgg/trends/data.html. Accessed 16 June 2019.
3. D. Archer *et al*., Atmospheric lifetime of fossil fuel carbon dioxide. *Annu. Rev. Earth Planet. Sci.* **37**, 117–134 (2009).
4. F. S. Zeman, K. S. Lackner, Capturing carbon dioxide directly from the atmosphere. *Glob. Warm. Int. Ctr. M.* **16**, 157–172 (2004).
5. T. E. Rufford *et al*., The removal of CO2 and N2 from natural gas: A review of conventional and emerging process technologies. *J. Petrol. Sci. Eng.* **94**, 123–154 (2012).
6. M. Ramezan *et al*., "Carbon dioxide capture from existing coal-fired power plants" (National Energy Technology Laboratory, DOE/NETL Report 401/110907, 2007).
7. C. M. White, B. R. Strazisar, E. J. Granite, J. S. Hoffman, H. W. Pennline, Separation and capture of CO2 from large stationary sources and sequestration in geological formations—Coalbeds and deep saline aquifers. *J. Air Waste Manage.* **53**, 645–715 (2003).
8. G. T. Rochelle, Amine scrubbing for CO2 capture. *Science* **325**, 1652–1654 (2009).
9. National Academies of Sciences, Engineering, and Medicine, *Negative Emissions Technologies and Reliable Sequestration: A Research Agenda* (National Academies Press, 2019).
10. R. Miner, B. Upton, Methods for estimating greenhouse gas emissions from lime kilns at Kraft pulp mills. *Energy* **27**, 729–738 (2002).
11. J.-W. Kim, H.-G. Lee, Thermal and carbothermic decomposition of Na 2 CO 3 and Li 2 CO 3. *Metall. Mater. Trans., B, Process Metall. Mater. Proc. Sci.* **32**, 17–24 (2001).
12. D. W. Keith, M. Ha-Duong, J. K. Stolaroff, Climate strategy with CO 2 capture from the air. *Climatic Change* **74**, 17–45 (2006).
13. D. W. Keith, G. Holmes, D. S. Angelo, K. Heidel, A process for capturing CO2 from the atmosphere. *Joule* **2**, 1573–1594 (2018).
14. D. W. Keith, Why capture CO2 from the atmosphere? *Science* **325**, 1654–1655 (2009).
15. B. Xu, Y. Bhawe, M. E. Davis, Low-temperature, manganese oxide-based, thermochemical water splitting cycle. *Proc. Natl. Acad. Sci. U.S.A.* **109**, 9260–9264 (2012).
16. L. Brecher, S. Spewock, C. Warde, The Westinghouse sulfur cycle for the thermochemical decomposition of water. *Int. J. Hydrogen Energ.* **2**, 7–15 (1977).
17. G. Beghi, A decade of research on thermochemical hydrogen at the joint research Centre Ispra. *Int. J. Hydrogen Energ.* **11**, 761–771 (1986).
18. P. Kaiser, R. B. Unde, C. Kern, A. Jess, Production of liquid hydrocarbons with CO2 as carbon source based on reverse water-gas shift and Fischer-Tropsch synthesis. *Chem-Ing-Tech* **85**, 489–499 (2013).
19. C.-S. Chen, W.-H. Cheng, S.-S. Lin, Mechanism of CO formation in reverse water–gas shift reaction over Cu/Al 2 O 3 catalyst. *Catal. Lett.* **68**, 45–48 (2000).
20. S. G. Jadhav, P. D. Vaidya, B. M. Bhanage, J. B. Joshi, Catalytic carbon dioxide hydrogenation to methanol: A review of recent studies. *Chem. Eng. Res. Des.* **92**, 2557–2567 (2014).
21. H. Yang *et al*., A review of the catalytic hydrogenation of carbon dioxide into value-added hydrocarbons. *Catal. Sci. Technol.* **7**, 4580–4598 (2017).
22. A. Steinfeld, Solar thermochemical production of hydrogen—A review. *Sol. Energy* **78**, 603–615 (2005).
23. M. Romero, A. Steinfeld, Concentrating solar thermal power and thermochemical fuels. *Energy Environ. Sci.* **5**, 9234–9245 (2012).
24. J. Schlaich, R. Bergermann, W. Schiel, G. Weinrebe, Design of commercial solar updraft tower systems—Utilization of solar induced convective flows for power generation. *Annu. Rev. Earth Planet. Sci.* **127**, 117–124 (2005).
25. A. Coustou, P. Alary, "Air power generator tower." US Patent 0199668A1 (2010).
26. A. R. Kulkarni, D. S. Sholl, Analysis of equilibrium-based TSA processes for direct capture of CO2 from air. *Ind. Eng. Chem. Res.* **51**, 8631–8645 (2012).
27. Y. Tian, C.-Y. Zhao, A review of solar collectors and thermal energy storage in solar thermal applications. *Appl. Energy* **104**, 538–553 (2013).
28. P. Furler *et al*., Solar thermochemical CO2 splitting utilizing a reticulated porous ceria redox system. *Energy Fuels* **26**, 7051–7059 (2012).
29. D. Graf, N. Monnerie, M. Roeb, M. Schmitz, C. Sattler, Economic comparison of solar hydrogen generation by means of thermochemical cycles and electrolysis. *Int. J. Hydrogen Energ.* **33**, 4511–4519 (2008).
30. Q. Feng, H. Kanoh, K. Ooi, Manganese oxide porous crystals. *J. Mater. Chem.* **9**, 319–333 (1999).
31. G. Gomori, Preparation of buffers for use in enzyme studies. *Method Enzymol.*, **1**, 138–146 (1955).
32. Y. Omomo, T. Sasaki, M. Watanabe, Preparation of protonic layered manganates and their intercalation behavior. *Solid State Ion.* **151**, 243–250 (2002).
33. B. D. James, D. A. DeSantis, G. Saur, "Hydrogen production pathways cost analysis (2013–2016)" (Strategic Analysis Inc., Arlington, VA, DOE-StrategicAnalysis-6231-1, 2016).
34. P. Rao, M. Muller, Industrial oxygen: Its generation and use" in *ACEEE Summer Study on Energy Efficiency in Industry* (American Council for an Energy-Efficient Economy, Washington, DC, 2007), pp. 124–135.
35. US Department of Energy, Energy Information Administration, "Electric Power Monthly, June 2019" (US Department of Energy, Washington, DC, https://www.eia.gov/electricity/monthly/archive/june2019.pdf).
36. T. Mancini *et al*., Dish-Stirling systems: An overview of development and status. *J. Sol. Energ.* **125**, 135–151 (2003).